Contemporary Engineering Sciences, Vol. 17, 2024, no. 1, 17 - 34
HIKARI Ltd, www.m-hikari.com
https://doi.org/10.12988/ces.2024.93125

Detection of Pneumonia in Children Aged 1 to 5 Years Using Transfer Learning and Deep Learning

B. Luna-Benoso

Instituto Politécnico Nacional. Escuela Superior de Cómputo
Av. Juan de Dios Bátiz, esq. Miguel Othón de Mendizábal
Mexico City 07738, Mexico

J.C. Martínez-Perales

Instituto Politécnico Nacional. Escuela Superior de Cómputo
Av. Juan de Dios Bátiz, esq. Miguel Othón de Mendizábal
Mexico City 07738, Mexico

L. Chavarria-Baez

Instituto Politécnico Nacional. Escuela Superior de Cómputo
Av. Juan de Dios Bátiz, esq. Miguel Othón de Mendizábal
Mexico City 07738, Mexico

U. S. Morales-Rodríguez

Instituto Politécnico Nacional. Escuela Superior de Cómputo
Av. Juan de Dios Bátiz, esq. Miguel Othón de Mendizábal
Mexico City 07738, Mexico

Abstract

Pneumonia is a respiratory tract infection and the leading cause of death in children between 1 and 5 years old. Qualified radiologists are responsible for diagnosing pneumonia in chest X-rays; however, deep learning techniques have shown favorable

results in developing computer-aided diagnosis systems that allow for the automatic detection of respiratory diseases such as pneumonia and can support specialists. This work proposes detecting pneumonia in chest X-rays of children under 5 years old using Transfer Learning applied to 5 Deep Learning models: DenseNet, ResNet, MobileNet, Inception V3, and EfficientNet. The models were compared using the metrics of $Accuracy$, $Sensitivity$, $Specificity$, and $Precision$ obtained from the confusion matrix of each model. The model that showed the best results was DenseNet, with the following metric values: $Accuracy = 90.4\%$, $Sensitivity = 0.95$, $Specificity = 0.83$, and $Precision = 0.90$.

Keywords: Deep Learning, Transfer Learning, DenseNet, ResNet, MobileNet, Inception V3, EfficientNet, and Pneumonia

1. Introduction

Pneumonia is a common respiratory tract infection affecting the lungs and mainly occurs in the elderly and children [1]. It is categorized based on where the infection was acquired; it can be community-acquired or hospital-acquired pneumonia, with Streptococcus pneumoniae being the primary cause of community-acquired pneumonia [2]. Pneumonia is one of the leading causes of mortality and morbidity worldwide. Before the COVID-19 era, there were over two million deaths annually worldwide [3]. For example, in the United Kingdom, the incidence of pneumonia has been increasing, from 1.5 per 1,000 people per year in 2022 to 2.2 per 1,000 in 2017, making it the leading cause of hospital admission and the third leading cause of respiratory mortality [4]. Globally, pneumonia is one of the leading infectious causes of death in children. Most healthy children can naturally fight off an infection; however, immunocompromised children are at higher risk of contracting pneumonia. UN statistics show that in 2017, over 808,000 children under 5 years old died, indicating that 15% of all deaths in children under 5 were due to pneumonia [5]. For example, in the United States, annual outpatient visits due to pneumonia range from 16.9 to 22.4 per 1,000 children. Some symptoms in pediatric patients include chest pain, poor feeding, cough, difficulty breathing, vomiting, and diarrhea [6]. There are several ways to detect pneumonia, such as computed tomography, and pulse oximetry, but the most common method is through radiographic evidence of new consolidation [7, 8]. However, in developing countries, timely detection of pneumonia in infants is concerning. In these countries, computer-aided diagnosis (CAD) systems are used due to their lower operational costs [9]. Although qualified radiologists usually diagnose pneumonia through chest X-rays (CXR), errors are common, generating false negatives. Hence, for analyzing difficult images, a hybridization between the radiologist and CAD systems is performed [7, 9].

Deep learning techniques have shown favorable results in developing CAD systems that enable the automatic detection of respiratory diseases [10]. Deep learning models require large amounts of data for training. However, nowadays, the transfer learning technique is used to avoid working with large datasets. For this, a deep learning model is trained using a large dataset and then the weights are transferred to train another model for new tasks to be classified using a smaller training dataset [9]. This work proposes detecting pneumonia in X-ray images of children under 5 years old using transfer learning and five deep learning models: DenseNet121, ResNet, EfficientNet, Inception, and MobileNet. The model results are compared using the confusion matrix and metrics such as $Accuracy$, $Sensitivity$, $Specificity$ and $Precision$.

2. Literature review

Pneumonia is one of the severe diseases affecting the lungs, causing significant human losses worldwide. Therefore, it is essential to have CAD systems capable of detecting pneumonia [11]. Various machine learning (ML) techniques have been employed for this purpose, such as using SVM to detect pneumonia caused by COVID-19 [12] in RGB images of CXR, or using texture features to feed classifier algorithms like K-NN, SVM, and Random Forest [13]. Other studies have used the histogram of oriented gradients (HOG) and local binary pattern (LBP) to extract features from CXR and subsequently used classifiers such as Random Forest, SVM, XGBoost, Decision Trees, Naïve Bayes, AdaBoost, K-NN, Logistic Regression, and Ensemble Model [14]. Furthermore, some studies use deep learning techniques for feature extraction, such as VGG16, which feeds into classifiers based on neural networks, SVM, KNN, Random Forest, and Naïve Bayes [8]. Other research utilizes deep learning to detect pneumonia caused by COVID-19 in CT scans and X-ray images [15], while other studies detect COVID-19 pneumonia using deep learning applied to lung ultrasound images [16]. Additionally, some research employs deep learning but transfers knowledge from a large pre-trained network to a smaller network using distillation techniques [10], and others use convolutional neural network (CNN) architectures with dropout layers carefully placed in the convolutional part of the network [17] instead of using distillation or transfer learning techniques. Transfer learning do researchers frequently use a technique today, alleviating the need for large amounts of data for deep learning training. For instance, some studies use transfer learning for pneumonia detection in CXR images aided by feature selection techniques based on particle swarm optimization [9]. Others use transfer learning to segment and detect pneumonia in CXR images using architectures like ResNet50, InceptionV3, and InceptionResNetV2 [18]. Some works focus on diagnosing pneumonia in children using single-channel photoplethysmography and employ ML algorithms such as Fine Decision Tree, Linear Discriminant Analysis, Weighted K Nearest Neighbors, Wide Neural Network, and

Ensemble of Bagged [19]. Other studies use deep learning with CNNs applied to CXR radiographs [20], and some combine deep learning with transfer learning [21].

3. Methodology

3.1 Convolutional Neural Networks (CNN)

Artificial Neural Networks (ANNs) are computational models inspired by the functioning of biological neural networks. They enable a training process where the weights of the network are adjusted to produce the desired output data, aiming to perform classification tasks. The simplest ANN model is known as the Single Perceptron. On the other hand, the Multilayer Perceptron (MLP), the most general

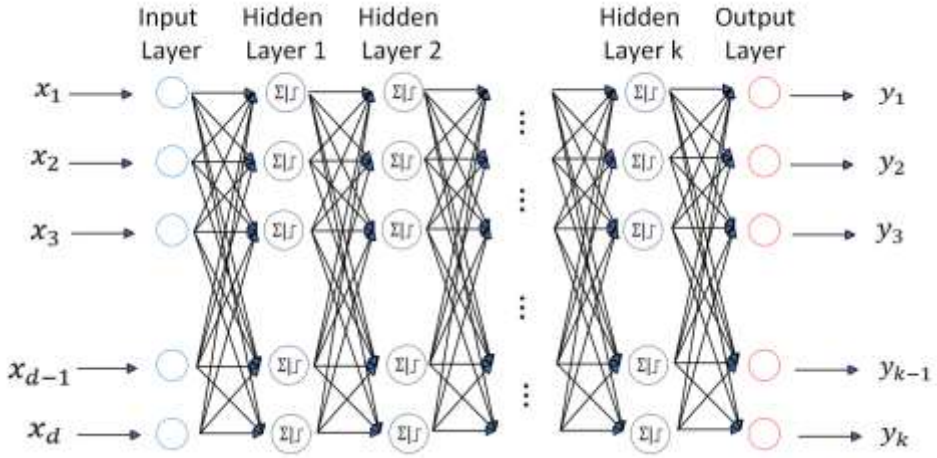

model, consists of an input layer, hidden layers, weighted connections, an activation function, and an output layer. Each layer is fully connected, and the training is conducted through backpropagation. Figure 1 shows the general model of MLP [22].

Fig. 1. Architecture of MLP with k hidden layers

Its three main types of layers characterize a CNN: convolutional layer, pooling layer, and fully connected (FC) layer. The convolutional layer is the first layer of a CNN and requires input data, a kernel, and a feature map. The pooling layer's task is to reduce dimensionality, and the fully connected layer is responsible for the classification process based on the features extracted in the previous layers. The main applications of CNNs are found in image recognition in computer vision [23], audio processing [24], and object segmentation [25]. Figure 2 shows the general architecture of a CNN.

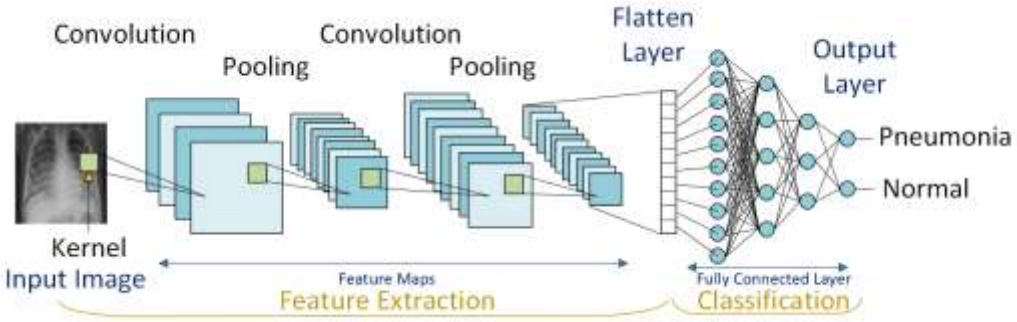

Fig. 2. Architecture of a CNN.

As the number of network layers increases in traditional CNN models, they tend to suffer from the vanishing gradient problem. To address this issue, Residual Networks, or more commonly known as ResNet, were introduced.

3.2 Residual Networks (ResNet)

ResNet is a deep learning model widely used in image classification that introduces the concept of skip connections to move over a set of layers. This is achieved through the implementation of so-called blocks. ResNet comprises residual and convolutional blocks. The identity block is used when the input and output have the same dimensions, and the convolutional block is used when the input and output dimensions are different. Figure 3
shows the structure of a residual block, where the arrow indicates the data flow, ReLU is the activation function, x is the input data to the block, and $f(x) + x$ is the output data [26].

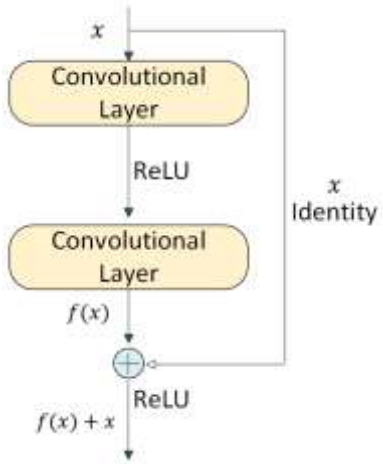

Fig. 3. Structure of a residual block

3.3 Densely Connected Convolutional Networks (DenseNet)

DenseNet is a CNN architecture composed of densely interconnected blocks chained sequentially. Each layer is connected to its subsequent layers within each block, and the blocks are interspersed with transition layers. Each dense block consists of multiple densely connected convolutional layers [27]. Figure 4 shows the architecture of DenseNet.

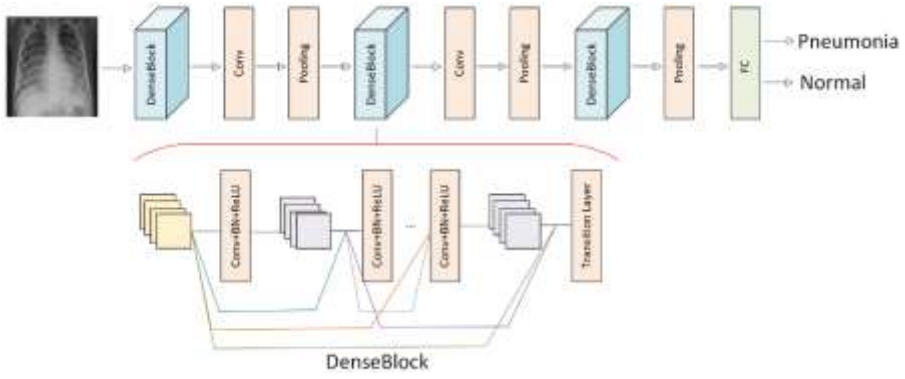

Fig. 4. DenseNet architecture.

3.4 Efficient Convolutional Neural Networks for Mobile Vision Applications (MobileNet)

MobileNet is a CNN designed primarily for mobile and embedded applications. It uses depth-wise separable convolutions to build deep and lightweight neural networks, significantly reducing the number of parameters compared to a CNN with regular convolutions of the same depth. A depth-wise separable convolution comprises two convolution operations: depth-wise convolution, which filters the input, and point-wise convolution 1×1, which receives the filtered values and creates new features [28]. MobileNet uses batch normalization (BN), which adds an additional step between neurons and the activation function to normalize the output. Figure 5 shows the comparison between using standard convolution and depth-wise separable convolution with ReLU activation layers.

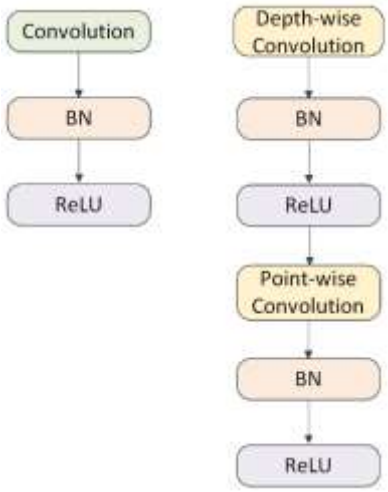

Fig. 5. Standard convolution (left) vs Depth-wise separable convolution (right) with ReLU activation layers.

3.5 Inception V3

Inception V3 is a CNN from the Inception family widely used in computer vision tasks. It uses blocks with multiple filters of different sizes at the same level, then concatenates them to extract features at different scales. Inception V3 shows improvements in the optimizer, loss function, and the addition of BN compared to its predecessors [29]. Figure 6 shows the architecture of Inception V3.

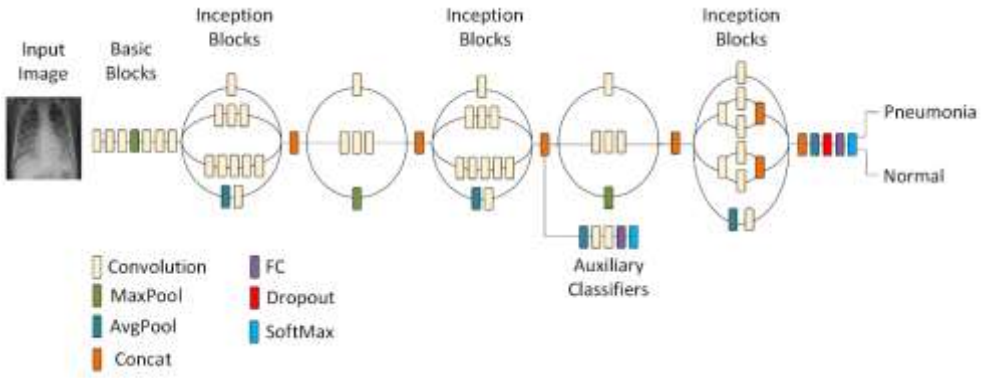

Fig. 6. Inception V3 architecture.

3.6 Rethinking Model Scaling for Convolutional Neural Networks (EfficientNet)

EfficientNet is a CNN that uses a compound scaling coefficient across all dimensions of depth, width, and resolution, scaling them uniformly using a set of fixed scaling

coefficients to optimize accuracy and efficiency relative to its size. Depth scaling involves adding more convolution layers to the convolution blocks, width scaling involves increasing the filters in the convolution layers, and resolution scaling involves increasing the input image size. Figure 7 shows the difference between a standard CNN and EfficientNet [30].

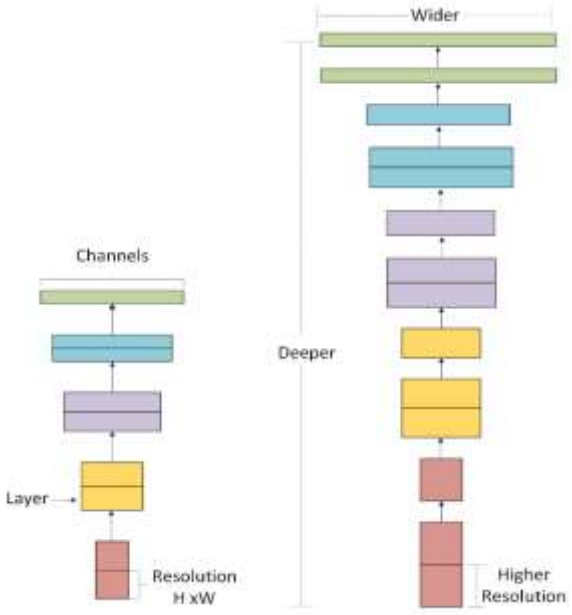

Fig. 7. Different types of CNN scaling. Standard convolution (left) vs EfficientNet (right).

3.7 Transfer Learning

Transfer learning is a machine learning technique that involves using part of the knowledge from previously trained models for a specific task as a starting point for developing other models with new tasks [31]. To use transfer learning, one needs to download the weights of the pre-trained network, replace the fully connected layer responsible for the classification process with the fully connected layer for the new task, and finally retrain the network. Figure 8 shows the concept of transfer learning.

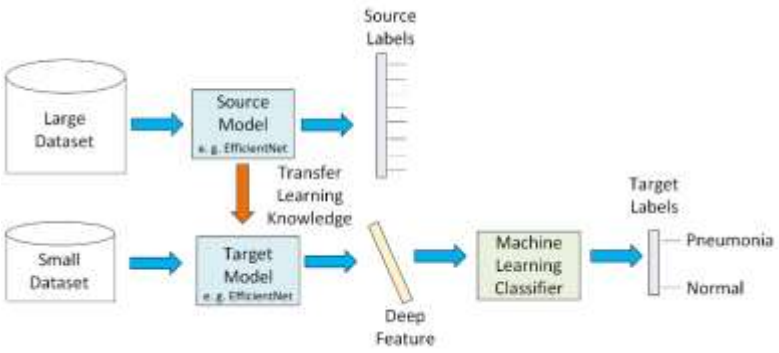

Fig. 8. Concept of Transfer Learning.

3.8 Confusion Matrix

The purpose of a confusion matrix is to evaluate the performance of a classifier model by describing how the actual values are distributed relative to the values output by the classifier model. Figure 9 shows a confusion matrix, grouping true positives (TP), true negatives (TN), false positives (FP), and false negatives (FN) that the model produces as results.

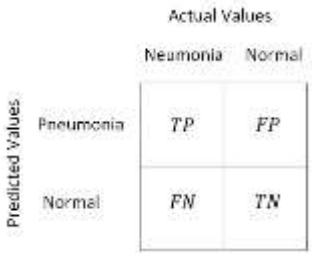

Fig. 9. Confusion matrix.

From the confusion matrix, the following metrics can be obtained [32]:

$Sensitivity$ (SE). Indicates the proportion of positive cases that a model correctly classifies.

$$SE = \frac{TP}{TP + FN}$$

$Specificity$ (SP). Indicates the model's ability to predict negative cases.

$$SP = \frac{TN}{TN + FP}$$

$Precision.$ Measures the proportion of relevant instances among the retrieved instances, calculated by the ratio of true positive predictions to all actual positive facts.

$$Precision = \frac{TP}{TP + FP}$$

$Accuracy$ (ACC). Represents the proportion of correct predictions, measuring how well a classification predicts a condition.

$$ACC = \frac{TN + TP}{FN + FP + TN + TP}$$

4. Experiments and Results

For the experimental part, the Chest X-ray Images (Pneumonia) dataset available at https://www.kaggle.com/datasets/paultimothymooney/chest-xray-pneumonia was used. This dataset consists of 5,862 chest X-ray images of pediatric patients aged one to five years from the Guangzhou Women and Children's Medical Center. The dataset is divided into two categories: pneumonia and normal. The chest X-rays were taken as part of routine clinical care, and the images were carefully reviewed by two medical experts. For the experimental development, deep learning was used with five models: DenseNet121, ResNet, EfficientNet, Inception V3, and MobileNet. Each model was trained using an 80% train-test split, with 80% for the training set and 20% for the test set. In total, 16 complete training sessions were carried out using optimizers such as Adagrad and Adam. To determine the hyperparameters that yield the minimum error function, different values for the learning rate were chosen, varying between a range of 0.00001 and 0.001. Figure 10 shows the 16 training sessions conducted with the DenseNet121 model.

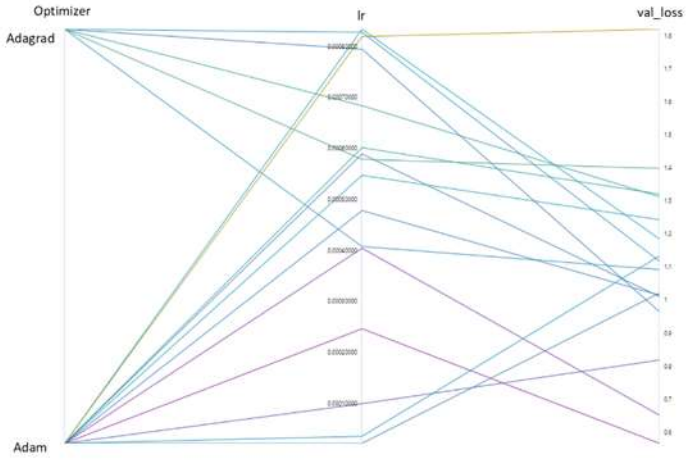

Fig. 10. DenseNet121 model training for hyperparameter selection.

The results in Figure 10 show that the best results are obtained using the Adam optimizer with a learning rate of 0.0002. Therefore, when using DenseNet121, the following hyperparameters were used:

- Image rescaling: $256px \times 256px$.
- Model type: binary (pneumonia/normal)).
- Classifier: sequential.
- Activation function: ReLU.
- Optimizer: Adam.
- Learning Rate: 0.0002.
- Epochs: 100.
- Loss function: binary cross-entropy.
- Convergence detection: early stopping.

With this set of parameters, the loss function for the DenseNet121 model was 0.3091. Figure 11 shows the results of the confusion matrix and the values of the metrics SE, SP, $Precision$, and ACC for the DenseNet121 model.

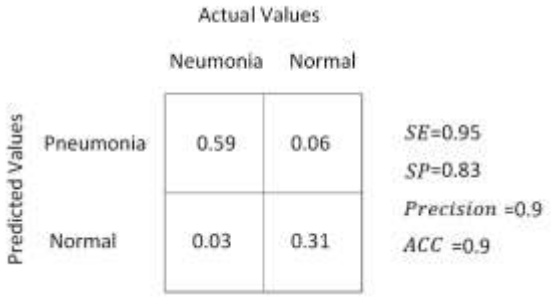

Fig. 11. Confusion matrix for the DenseNet121 model.

Similarly, experiments were conducted for the ResNet, EfficientNet, Inception V3, and MobileNet architectures with the Adam and Adagrad optimizers. Figure 12 shows the training results of the four models with the Adam and Adagrad optimizers.
Inception V3—achieves better results when using the Adagrad optimizer with learning rates of 0.0004, 0.0003, 0.0003, and 0.0009, respectively.
Figure 13 shows the resulting confusion matrix for the ResNet, EfficientNet, MobileNet, and Inception V3 models when using the following hyperparameters:

- Image rescaling: $256px \times 256px$.
- Model type: binary (pneumonia/normal).
- Classifier: sequential.
- Activation function: ReLU.
- Optimizer: Adam.
- Epochs: 100.

- Loss function: binary cross-entropy.
- Convergence detection: early stopping.

and the respective learning rates obtained from Figure 12.

Fig. 12. Training of ResNet, EfficientNet, MobileNet, and Inception V3 models with Adam and Adagrad optimizers.

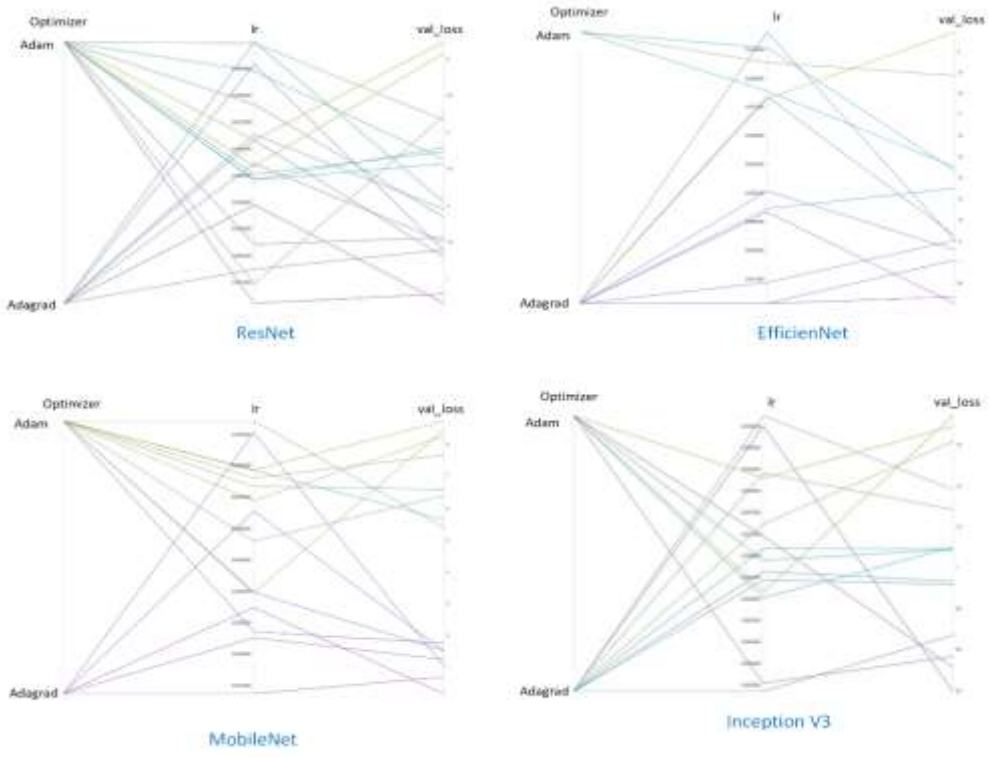

From Figure 12, it is inferred that each model—ResNet, EfficientNet, MobileNet, and Table 1 shows the comparison of the models of the five architectures used in this work and the values of the SE, SP, $Precision$, ACC metrics, and the loss function value.

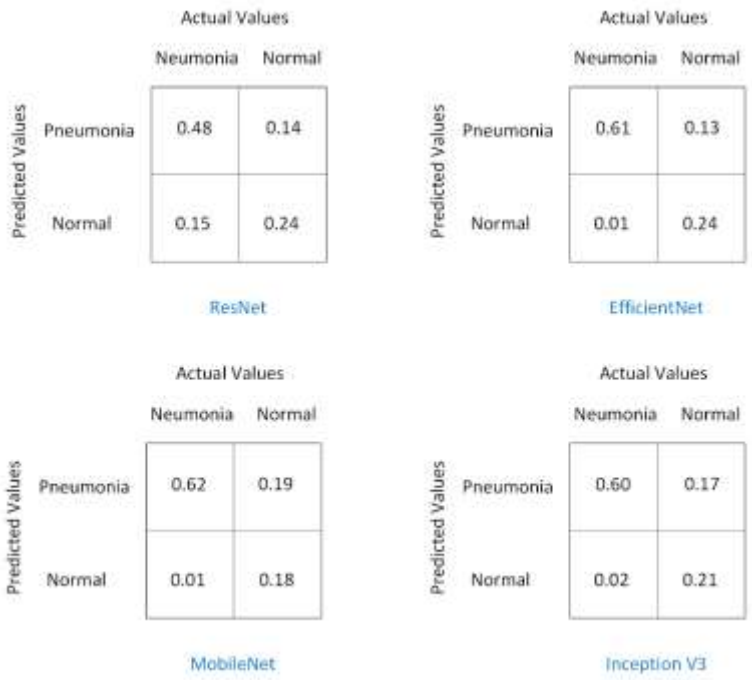

Fig. 13 Confusion matrix resulting from using ResNet, EfficientNet, MobileNet and Inception V3.

Model	*SE*	*SP*	*Precision*	*ACC*	*Loss*
DenseNet121	0.95	0.83	0.90	**90.4**%	0.3091
EfficientNet	0.98	0.64	0.82	**85.4**%	0.6069
Inception V3	0.96	0.55	0.77	**81.4**%	0.5188
MobileNet	0.98	0.48	0.76	**80.0**%	0.5904
ResNet	0.76	0.63	0.77	**71.8**%	0.5439

Table 1. Comparison of different metrics applied to the five models.

5. Conclusions

In this work, five Deep Learning models were presented and applied to the problem of detecting pneumonia in children under 5 years old using the Chest X-ray Images (Pneumonia) dataset obtained from Kaggle. The dataset consists of chest X-rays of patients with pneumonia and healthy patients, divided into two categories: pneumonia and normal. The models applied were DenseNet121, EfficientNet, Inception V3, MobileNet, and ResNet. DenseNet showed the best results in hyperparameter

configuration using the Adam optimizer, while the rest of the models showed better results with the Adagrad optimizer. Figures 11 and 13 show the confusion matrix results for each model, and Table 1 compares the five models using metrics obtained from the confusion matrix such as $Sensitivity$, $Specificity$, $Precision$, and $Accuracy$, as well as the loss function value for each model. A $Sensitivity$ value closer to 1 indicates a reduction in false negatives. Although EfficientNet, Inception V3, and MobileNet achieved higher $Sensitivity$ values (0.98, 0.96, and 0.98 respectively) compared to DenseNet121 (0.95), the $Specificity$, $Precision$, and $Accuracy$ values were better for DenseNet121. $Specificity$ values closer to 1 indicate a reduction in false positives. DenseNet121 achieved a $Specificity$ value of 0.83 and an $Accuracy$ of 90.4%, the best results compared to the other models. Additionally, the loss function yielded the lowest value with DenseNet121 at 0.3091, quantifying the discrepancy between the model's predicted values and the actual values. This work concludes that Transfer Learning with the DenseNet121 model yields the best results compared to the models proposed in Table 1 for detecting pneumonia in chest X-rays of children under 5 years old.

Acknowledgments. The authors would like to thank the Instituto Politécnico Nacional (Secretaría Académica, COFAA, EDD, EDI, SIP, and ESCOM) and CONAHCYT for their financial support in developing this work.

References

[1] Zhen, J.; Wang, J.; Tang, L.; Ma, Y.; Tian, Y. Association of residential greenness with incident pneumonia: A prospective cohort study, *Science of the Total Environment*, **940** (2024), 173731. https://doi.org/10.1016/j.scitotenv.2024.173731

[2] Lv, M.; Du, J.; Xie, M. Z.; Zhou, Y.; Yang, G.; Wang, J.; Zhang, W. X.; Yang, H.; Zhang S. S.; Cui, F.; Lu Q. B.; Wu, J. Protective effect of PCV13 against all-cause hospitalized pneumonia in children in Beijing, China: real-world evidence, *Vaccine,* **42** (2024), no. 12, 3091-3098. https://doi.org/10.1016/j.vaccine.2024.04.015

[3] Rögnvaldsson, K. G.; Bjarnason, A.; Olafsdóttir, I. S.; Helgason, K. O.; Guðmundsson, A.; Gottfreðsson, M. Adults with symptoms of pneumonia: a prospective comparison of patients with and without infiltrates on chest radiography, *Clinical Microbiology and Infection*, **29** (2023), no. 1,108.e1-108.e6. https://doi.org/10.1016/j.cmi.2022.07.013

[4] Pates, K. M.; Periselneris, J. N.; Brown, J. S. Pneumonia, *Medicine,* **51** (2023), no. 11, 763-767. https://doi.org/10.1016/j.mpmed.2023.08.003

[5] WHO. *World Health Organization*. Ultimo Acceso: julio de 2024. https://www.who.int/health-topics/pneumonia#tab=tab_1

[6] Gottlieb, M.; Heinrich, S. A. How Reliable Are Signs and Symptoms for Diagnosing Pneumonia in Pediatric Patients?. *Annals of Emergency Medicine*, **71** (2018), no. 6, 725-727. https://doi.org/10.1016/j.annemergmed.2017.09.028

[7] Nalluri, S.; Sasikala, R. Pneumonia screening on chest X-rays with optimized ensemble model, *Expert Systems with Applications*, **242** (2024), 122705. https://doi.org/10.1016/j.eswa.2023.122705

[8] Sharma, S.; Guleria, K. A Deep Learning based model for the Detection of Pneumonia from Chest X-Ray Images using VGG-16 and Neural Networks, *Procedia Computer Science*, **218** (2023), 357-366. https://doi.org/10.1016/j.procs.2023.01.018

[9] Pramanik, R.; Sarkar, S.; Sarkar, R. An adaptive and altruistic PSO-based deep feature selection method for Pneumonia detection from Chest X-rays, *Applied Soft Computing*, **128** (2022), 109464. https://doi.org/10.1016/j.asoc.2022.109464

[10] Kabir, M.; Mridha, M. F.; Rahman, A.; Hamid, A.; Monowar, M. M. Detection of COVID-19, pneumonia, and tuberculosis from radiographs using AI-driven knowledge distillation, *Heliyon*, **10** (2024), e26801. https://doi.org/10.1016/j.heliyon.2024.e26801

[11] Kareem, A.; Liu, H.; Velisavljevic, V. A federated learning framework for pneumonia image detection using distributed data, *Healthcare Analytics*, **4** (2023), 100204. https://doi.org/10.1016/j.health.2023.100204

[12] Absar, N.; Mamur, B.; Mahmud, A.; Emran, T. B.; Khandaker, M. U.; Faruque, M. R. I.; Osman, H.; Elzaki, A.; Elkhader, B. A. Development of a computer-aided tool for detection of COVID-19 pneumonia from CXR images using machine learning algorithm, *Journal of Radiation Research and Applied Sciences*, **15** (2022), 32-43. https://doi.org/10.1016/j.jrras.2022.02.002

[13] Ortiz-Toro, C.; García-Pedrero, A.; Lillo-Saavedra, M.; Gonzalo-Martín, C. Automatic detection of pneumonia in chest X-ray images using textural features, *Computers in Biology and Medicine*, **145** (2022), 105466. https://doi.org/10.1016/j.compbiomed.2022.105466

[14] Amin, A. U.; Taj, S.; Hussain, A.; Seo, S. An automated chest X-ray analysis for COVID-19, tuberculosis, and pneumonia employing ensemble learning approach. *Biomedical Signal Processing and Control*, **87** (2024), 105408. https://doi.org/10.1016/j.bspc.2023.105408

[15] Kumar, A. RYOLO v4-tiny: A deep learning based detector for detection of COVID and Non-COVID Pneumonia in CT scans and X-RAY images, *Optik - International Journal for Light and Electron Optics*, **268** (2022), 169786. https://doi.org/10.1016/j.ijleo.2022.169786

[16] La Salvia, M.; Secco, G.; Torti, E.; Florimbi, G.; Guido, L.; Lago, P.; Salinaro, F.; Perlini, S.; Leporati, F. Deep learning and lung ultrasound for Covid-19 pneumonia detection and severity classification, *Computers in Biology and Medicine*, **136** (2021), 104742. https://doi.org/10.1016/j.compbiomed.2021.104742

[17] Szepesi, P.; Szilágyi, L. Detection of pneumonia using convolutional neural networks and deep learning, *Biocybernetics and Biomedical Engineering*, **42** (2022), 1012-1022. https://doi.org/10.1016/j.bbe.2022.08.001

[18] Manickam, A.; Jiang, J.; Zhou, Y.; Sagar, A.; Soundrapandiyan, R.; Dinesh, J. S. Automated pneumonia detection on chest X-ray images: A deep learning approach with different optimizers and transfer learning architectures, *Measurement*, **184** (2021), 109953. https://doi.org/10.1016/j.measurement.2021.109953

[19] Kanwal, K.; Khalid, S. G.; Asif, M.; Zafar, F.; Qurashi, A. G. Diagnosis of Community-Acquired pneumonia in children using photoplethysmography and Machine learning-based classifier, *Biomedical Signal Processing and Control*, **87** (2024), 105367. https://doi.org/10.1016/j.bspc.2023.105367

[20] Rifai, A. M.; Raharjo, S.; Utami, E.; Ariatmanto, D. Analysis for diagnosis of pneumonia symptoms using chest X-ray based on MobileNetV2 models with image enhancement using white balance and contrast limited adaptive histogram equalization (CLAHE), *Biomedical Signal Processing and Control*, **90** (2024), 105857. https://doi.org/10.1016/j.bspc.2023.105857

[21] Arun, P. J.; Asswin, C. R.; Dharshan, K. K. S.; Avinash, D.; Vinayakumar, R.; Sowmya V.; Gopalakrishnan, E. A.; Soman, K. P. Transfer learning approach for pediatric pneumonia diagnosis using channel attention deep CNN architectures, *Engineering Applications of Artificial Intelligence*, **123** (2023), 106416. https://doi.org/10.1016/j.engappai.2023.106416

[22] Liu, W.; Zhang, L.; Xie, L.; Hu, T.; Li, G.; Bai, S.; Yi, Z. Multilayer perceptron neural network with regression and ranking loss for patient-specific quality assurance, *Knowledge-Based Systems*, **271** (2023), 110549. https://doi.org/10.1016/j.knosys.2023.110549

[23] Ding, W.; Luo, Y., Lin, Y.; Yang, Y.; Lian, S. Veri. Bypasser: An automatic image verification code recognition system based on CNN, *Computer Communications*, **217** (2024), 246-258. https://doi.org/10.1016/j.comcom.2023.12.022

[24] Wu, Y.; Hu, R.; Wang, X. Adaptive subband partition encoding scheme for multiple audio objects using CNN and residual dense blocks mixture network, *Expert Systems with Applications*, **247** (2024), 123323. https://doi.org/10.1016/j.eswa.2024.123323

[25] Sefti, R.; Sbibih, D.; Jennane, R. A CNN-based spline active surface method with an after-balancing step for 3D medical image segmentation, *Mathematics and Computers in Simulation*, **225** (2024), 607-618. https://doi.org/10.1016/j.matcom.2024.06.002

[26] Tang, X.; Shi, Y.; Lou, L.; Yu, J.; Fan, Z.; Lai, J.; Xiong, S. Multi-objective optimization model of Ultra-High Voltage Direct Current system considering low carbon and equipment safety based on Im-NSGA-II and ResNet-LSTM, *Computers and Electrical Engineering*, **118** (2024), 109441. https://doi.org/10.1016/j.compeleceng.2024.109441

[27] Xu, L.; Yang, J.; Ge, M.; Su, Z. Three-dimensional fatigue crack quantification using densely connected convolutional network-assisted ultrasonic guided waves, *International Journal of Fatigue*, **180** (2024), 108094. https://doi.org/10.1016/j.ijfatigue.2023.108094

[28] Shome, N.; Kashyap, R.; Laskar, R. H. Detection of tuberculosis using customized MobileNet and transfer learning from chest X-ray image, *Image and Vision Computing*, **147** (2024), 105063. https://doi.org/10.1016/j.imavis.2024.105063

[29] Khan, N.; Das, S.; Liu, J. Predicting pedestrian-involved crash severity using inception-v3 deep learning model, *Accident Analysis and Prevention*, **197** (2024), 107457. https://doi.org/10.1016/j.aap.2024.107457

[30] Nigama, S.; Jain, R.; Singh, V. K.; Marwaha, S.; Arora, A.; Jain, S. EfficientNet architecture and attention mechanism-based wheat disease identification model, *Procedia Computer Science*, **235** (2024), 383-393. https://doi.org/10.1016/j.procs.2024.04.038

[31] Zhou, J.; Gu, X.; Gong, H.; Yang, X.; Sun, Q.; Guo, L.; Pan, Y. Intelligent classification of maize straw types from UAV remote sensing images using DenseNet201 deep transfer learning algorithm, *Ecological Indicators*, **166** (2024), 112331. https://doi.org/10.1016/j.ecolind.2024.112331

[32] Valero-Carreras, D.; Alcaraz, J.; Landete, M. Comparing two SVM models through different metrics based on the confusion matrix, *Computers & Operations Research*, **152** (2023), 106131. https://doi.org/10.1016/j.cor.2022.106131

Received: July 23, 2024; Published: August 16, 2024